Inorg. Chem. **2005**, *44*, 3337–3346

Synthesis, Structural Characterization, and Magnetic Studies of Polynuclear Iron Complexes with a New Disubstituted Pyridine Ligand

Hayley A. Burkill,[†] Neil Robertson,[‡] Ramón Vilar,*[,§] Andrew J. P. White,[†] and David J. Williams[†]

Department of Chemistry, Imperial College London, South Kensington, London SW7 2AZ, United Kingdom, School of Chemistry, The University of Edinburgh, Joseph Black Building, West Mains Road, Edinburgh EH9 3JJ, United Kingdom, and ICREA and Institute of Chemical Research of Catalonia (ICIQ), 43007 Tarragona, Spain

Received October 4, 2004

A series of novel polyiron species have been prepared from the reaction of iron chloride with the 2,5-disubstituted pyridines $\mathbf{H_2L}^n$ ($\mathbf{H_2L^1}$ = *N*,*N*′-bis(*n*-butylcarbamoyl)pyridine-2,6-dicarboxamide; $\mathbf{H_2L^2}$ = *N*,*N*′-bis(*n*-ethylcarbamoyl)-pyridine-2,6-dicarboxamide). By small modifications of the experimental conditions under which the reactions are carried out, it has been possible to prepare the quadruply stranded diiron(II) complex $[Fe_2(\mu\text{-}\mathbf{H_2L^1})_4(\mu\text{-}Cl)_2][FeCl_4]_2$ (**1**), the metallamacrocycle $[Fe_2(\mu\text{-}\mathbf{H_2L^1})_2(THF)_4Cl_2][FeCl_4]_2$ (**2**), the hexairon(III) compound $[Fe_6(\mathbf{L^1})_2(\mu\text{-}OMe)_6(\mu_4\text{-}O)_2Cl_4]$ (**3**), and the mixed-valence trinuclear iron complexes $[Fe_3(\mathbf{L}^n)_3(\mu_3\text{-}O)]$ (n = 1, **4**; n = 2, **5**). The X-ray crystal structures of **3** and **5** and magnetic studies for all the compounds are herein presented. Interestingly, the structural analysis of **5** at room temperature indicates that one of the iron centers is Fe^{III} while the other two have an average valence state between Fe^{II} and Fe^{III}. The five complexes herein presented demonstrate the great versatility that the new ligand has as a building block for the formation of supramolecular coordination assemblies.

During the past few years supramolecular chemistry has seen the development of a wide range of methodologies for the synthesis of complex molecular architectures. To obtain these novel assemblies, coordination of specially designed ligands for metal centers has proven to be a very successful strategy.[1] This is partly due to the wide range of structural motifs offered by metal centers and also to the relative lability of the coordination bond in comparison to covalent bonds, which provides the possibility of "correcting" errors in the self-assembly process. Furthermore, metal centers can provide unique optical, magnetic, or catalytic properties to the assembly and, hence, materials with useful properties can be synthesized.

As part of our interest in preparing metalla-assemblies with ligands that contain hydrogen-bonding functionalities, we have recently synthesized $\mathbf{H_2L^1}$ (*N*,*N*′-bis(*n*-butylcarbamoyl)-pyridine-2,6-dicarboxamide) and investigated its reactions with iron salts.[2] In a preliminary communication we reported that in its neutral form this ligand can coordinate to two different iron(II) centers—via the oxygen atoms of the urea groups—to yield either the quadruply stranded helicate $[Fe_2(\mu\text{-}\mathbf{H_2L^1})_4(\mu\text{-}Cl)_2][FeCl_4]_2$ (**1**) or the metallamacrocycle $[Fe_2(\mu\text{-}\mathbf{H_2L^1})_2(THF)_4Cl_2][FeCl_4]_2$ (**2**) (see Chart 1). The deprotonation of the urea groups of $\mathbf{H_2L^1}$ to yield $\mathbf{[L^1]}^{2-}$ could provide yet another coordinating mode for this ligand with the potential to bind the metal center more tightly via the pyridine and amidato groups leaving one set of hydrogen-bonding moieties available for supramolecular interactions (see Scheme 1). Furthermore, the presence of several N- and O-coordinating sites on this ligand makes it particularly attractive for the preparation of polynuclear iron complexes, which are of great importance due to their unique magnetic

* Author to whom correspondence should be addressed. E-mail: rvilar@iciq.es. Telephone: +34 977 920 212. Fax: +34 977 920 228.
† Imperial College London.
‡ The University of Edinburgh.
§ ICREA and Institute of Chemical Research of Catalonia (ICIQ).

(1) See for example: (a) Seidel, S. R.; Stang, P. J. *Acc. Chem. Res.* **2002**, *35*, 972. (b) Ward, M. D.; McCleverty, J. A.; Jeffery, J. C. *Coord. Chem. Rev.* **2001**, *222*, 251. (c) Fujita, M.; Ogura, K. *Coord. Chem. Rev.* **1996**, *148*, 249. (d) Seidel, S. R.; Stang Peter, J. *Acc. Chem. Res.* **2002**, *35*, 972. (e) Fujita, M.; Umemoto, K.; Yoshizawa, M.; Fujita, N.; Kusukawa, T.; Biradha, K. *Chem. Commun.* **2001**, 509. (f) Fujita, M. *Acc. Chem. Res.* **1999**, *32*, 53. (g) Swiegers, G. F.; Malefetse, T. J. *Chem. Rev.* **2000**, *100*, 3483. (h) Saalfrank, R. W.; Uller, E.; Demleitner, B.; Bernt, I. *Struct. Bonding* **2000**, *96*, 149. (i) Caulder, Dana L.; Raymond, Kenneth N. *Acc. Chem. Res.* **1999**, *32*, 975.

(2) Burkill, H. A.; Vilar, R.; White, A. J. P.; Williams, D. J. *J. Chem. Soc., Dalton Trans.* **2002**, 837.

10.1021/ic048620e CCC: $30.25
Published on Web 04/07/2005

Chart 1. Representation of the Quadruply Stranded Helicate **1** and the Metallamacrocycle **2**

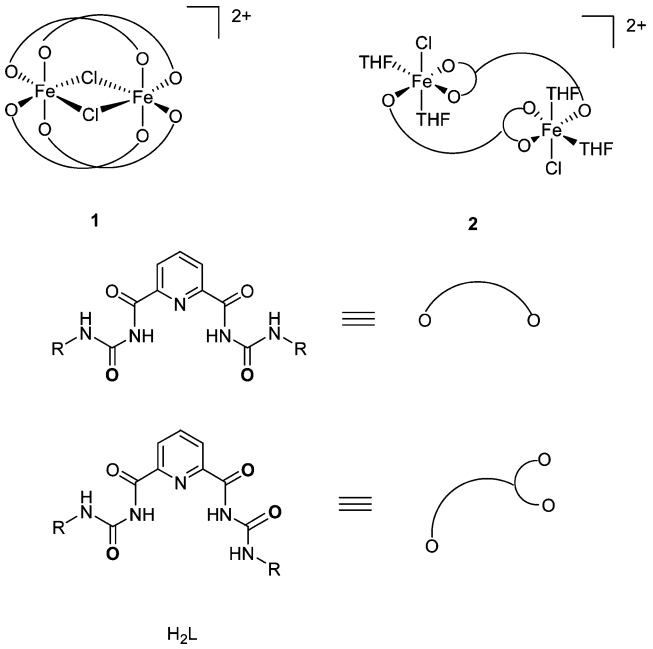

properties and to the important roles they play in biological systems. Diiron sites, for example, are essential for the dioxygen chemistry of several metalloenzymes such as hemerythrin, methane monoxygenase, and ribonucleotide reductase. Studying the structure and reactivity of such species in both the proteins and biomimetic models is of great interest to obtain a better understanding of the biological processes.

Herein we report the structural characterization of $\mathbf{H_2L^1}$ and the synthesis of the new hexairon compound $[Fe_6(\mathbf{L^1})_2(\mu\text{-OMe})_6(\mu_4\text{-O})_2Cl_4]$ (**3**) from the reaction between $\mathbf{H_2L^1}$ in the presence of NaH and iron chloride, methanol, and traces of water. In this reaction, the expected N,N′,N″ coordination of $\mathbf{[L^1]}^{2-}$ to iron is indeed observed (yielding the fragment $[Fe\mathbf{L^1}]^+$); however, this moiety reacts readily with traces of H_2O and methanol generating the hexanuclear complex **3**. To explore further this type of reaction $\mathbf{H_2L^n}$ ($n = 1$, R = Bu; $n = 2$, R = Et) was treated with DBU (1,8-diazabicyclico-[5.4.0]undec-7-ene) to remove the protons of the carboxamide groups and reacted with iron chloride (avoiding the presence of any alcohol as a solvent). Once again the expected N,N′,N″ tricoordinated iron complex was formed which proved to be reactive to traces of O_2 yielding the novel mixed-valence triiron complexes $[Fe_3(\mathbf{L^n})_3(\mu_3\text{-O})]$ ($n = 1$, R = Bu, **4**; $n = 2$, R = Et, **5**) one of which (R = Et) has been structurally characterized. Magnetic studies of the metalla-assemblies have also been carried out and are discussed in this paper.

Experimental Details

Although we have previously reported in a communication[2] the syntheses of $\mathbf{H_2L^1}$ and the diiron complexes **1** and **2**, herein we present a full and more detailed experimental procedure for their syntheses and characterization.

Synthesis of $\mathbf{H_2L^1}$ (*N*,*N*′-Bis(*n*-butylcarbamoyl)pyridine-2,6-dicarboxamide). A solution of butylurea (4.547 g, 39.19 mmol) in CH_2Cl_2 (50 mL) was added to a solution of 2,6-pyridinedicarbonyl dichloride (1.999 g, 9.79 mmol) in CH_2Cl_2 (30 mL). The resulting pale yellow solution was stirred overnight and then evaporated to dryness under reduced pressure to give a yellow oil. The oil was stirred vigorously with diethyl ether to give a white solid, which was washed with distilled water to remove excess butylurea. The crude product was recrystallized from CH_2Cl_2/diethyl ether to give a white solid. Yield: 2.68 g, 76%. Anal. Found: C, 56.11; H, 6.80; N, 19.12. Calcd for $C_{17}H_{25}N_5O_4$: C, 56.19; H, 6.93; N, 19.27. IR (ν_{max}/cm^{-1}, KBr): 3324 (N−H), 2960 (C−H), 2931 (C−H), 2863 (C−H) 1693 (bd, C═O), 1550 (C═N). ^{1}H NMR (δ_H; $CDCl_3$): 0.92 (t, 6H, H_a, $^3J_{HH} = 7.2$ Hz), 1.42, 1.57 (two multiplets, 8H, $H_{b,c}$), 3.33 (dt, 4H, H_d, $^3J_{HH} = 6.9$ Hz, $^3J_{HH} = 5.7$ Hz), 8.13 (t, 1H, H_h, $^3J_{HH} = 7.8$ Hz), 8.42 (d, 2H, H_g, $^3J_{HH} = 7.8$ Hz), 8.51 (t, 2H, H_e, $^3J_{HH} = 5.7$ Hz), 10.73 (s (bd), 2H, H_f). ^{13}C{^{1}H} NMR (δ_P; $CDCl_3$): 164.10 (C6), 153.80 (C5), 147.57 (C7), 139.72 (C8), 126.66 (C9), 39.69 (C4), 31.58 (C3), 20.15 (C2), 13.82 (C1). MS (FAB$^+$) (*m*/*z*): 364 {[M + H]$^+$}, 291 {[M − ($C_4H_{10}N$)]$^+$}, 218 {[M − ($C_8H_{22}N_2$)]$^+$}, 192 {[M − ($C_9H_{19}N_2O$)]$^+$}. MS (low-resolution electrospray)$^+$ (3.09×10^7 V) (*m*/*z*): 363 {[M + H]$^+$}, 727 {[2M + H]$^+$}. UV−vis (λ_{max} /nm): 270 (CH_3CN), 290 (THF). Extinction coefficient (ϵ_λ/M^{-1} cm^{-1}): 6.5×10^3 (CH_3CN), 2.2×10^3 (THF). Melting point 189−192 °C.

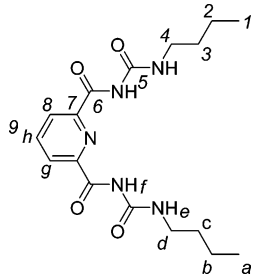

Synthesis of $\mathbf{H_2L^2}$ (*N*,*N*′-Bis(*n*-ethylcarbamoyl)pyridine-2,6-dicarboxamide). A solution of ethylurea (3.441 g, 39.10 mmol) in CH_2Cl_2 (45 mL) was added to a solution of 2,6 pyridinedicarbonyl dichloride (2.009 g, 9.85 mmol) in CH_2Cl_2 (30 mL). The resulting pale yellow solution was stirred overnight and then evaporated to dryness under reduced pressure to give a yellow oil. This was stirred vigorously with diethyl ether to give a white solid, which was washed with distilled water (4 × 20 mL) to remove excess ethylurea. The crude product was recrystallized from CH_2Cl_2/diethyl ether to give a white solid. Yield: 1.622 g, 54%. Anal. Found: C, 50.82; H, 5.71; N, 22.79. Calcd for $C_{13}H_{17}N_5O_4$: C, 50.81; H, 5.58; N, 22.79. IR (ν_{max}/cm^{-1}, KBr): 3324 (N−H), 2979

Scheme 1. Deprotonation of the Urea Groups Generating a Tridentate Ligand

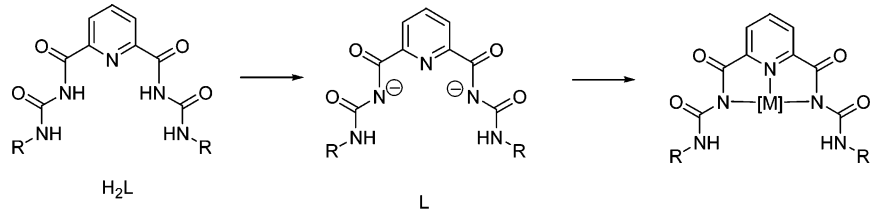

(C−H), 2900 (C−H), 1708 (C═O), 1544 (C═N). ^{1}H NMR (δ_H; $CDCl_3$): 1.21 (t, 6H, H_a, $^3J_{HH}$ = 7.3 Hz), 3.38 (dq, 4H, H_b, $^3J_{HH}$ = 7.2 Hz), 8.13 (t, 1H, H_f, $^3J_{HH}$ = 7.4 Hz), 8.42 (d, 2H, H_e, $^3J_{HH}$ = 7.9 Hz), 8.48 (t, 2H, H_c, $^3J_{HH}$ = 5.3 Hz), 10.70 (s (bd), 2H, H_d). ^{13}C{^{1}H} NMR (δ_C; $CDCl_3$): 164.38 (C3), 153.73 (C4), 147.91 (C5), 139.42 (C6), 126.67 (C7), 34.78 (C2), 14.86 (C1). MS (FAB$^+$) (*m*/*z*): 615 {[2M + H]$^+$}, 308 {[M + H]$^+$}, 263 {[M − (C_2H_7N)]$^+$}, 218 {[M − $C_4H_{14}N_2$]$^+$}.

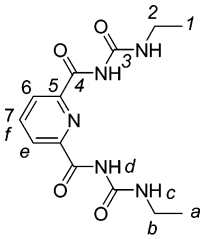

Synthesis of [Fe_2(μ-H_2L^1)$_4$(μ-Cl)$_2$][$FeCl_4$]$_2$ (1). A suspension of $FeCl_2$ (0.035 g, 0.28 mmol) in CH_2Cl_2 (10 mL) was added to a solution of H_2L^1 (0.217 g, 0.60 mmol) in CH_2Cl_2. The resulting cloudy suspension was stirred under nitrogen for ca. 3 h. To this was added a solution of $FeCl_3$ (0.048 g, 0.30 mmol) in CH_2Cl_2 (10 mL) upon which a color change from orange to yellow was observed. The yellow solution was stirred overnight, and upon precipitation with hexane, a yellow product was obtained. Single crystals suitable for X-ray analysis were obtained from a THF/hexane mixture. Yield: 0.231 g, 79%. Anal. Found: C, 40.95; H, 5.13; N, 13.52. Calcd for [$C_{68}H_{100}N_{20}O_{16}Cl_2Fe_2$][$FeCl_4$]$_2$·$C_4H_8O$: C, 41.11; H, 5.17; N, 13.32. IR (ν_{max}/cm^{-1}, KBr): 2960 (C−H), 2933 (C−H), 2873 (C−H), 1703 (C═O), 1661 (C═O), 1563 (C═N), 1429 (C−H), 381 ($FeCl_4^-$). Raman (ν_{max}/cm^{-1}): 332 ($FeCl_4^-$). MS-FAB(+) (*m*/*z*): 1834 {[M − $FeCl_4$]$^+$}, 1270 {[M − L − 2$FeCl_4$]$^+$}, 1308 {[M − L^1 − 2($FeCl_4$) + Cl]$^+$}, 907 {[M − 2L^1 − 2($FeCl_4$)]$^+$}. MS-FAB(−) (*m*/*z*): 198 {[$FeCl_4$]$^-$}, 163 {[$FeCl_3$]$^-$}.

Synthesis of [Fe_2(μ-H_2L^1)$_2$(THF)$_4$$Cl_2$][$FeCl_4$]$_2$ (2). A suspension of $FeCl_2$ (0.034 g, 0.27 mmol) in THF (10 mL) was added to a solution of H_2L^1 (0.215 g, 0.59 mmol) in THF to give a slightly cloudy orange solution. A solution of $FeCl_3$ (0.047 g, 0.29 mmol) in THF (10 mL) was then added upon which the solution lightened slightly in color and all the solid in the reaction mixture dissolved. The resulting orange solution was stirred under nitrogen for ca. 3 h. The volume was reduced under reduced pressure and the orange product **4** obtained by precipitation with hexane. Crystals suitable for X-ray analysis were obtained from a THF/hexane mixture. Yield: 0.119 g, 84%. Anal. Found: C, 34.34; H, 4.84; N, 9.62. Calcd for [$C_{42}H_{70}N_{10}O_{12}Cl_2Fe_2$][$FeCl_4$]$_2$: C, 33.97; H, 4.75; N, 9.43. IR (ν_{max}/cm^{-1}, KBr): 2960 (C−H), 2934 (C−H), 2873 (C−H), 1703 (C═O), 1663 (C═O), 1563 (C═N), 383 ($FeCl_4^-$). MS (FAB$^+$) (*m*/*z*): 1125 {[M − THF − 2($FeCl_4$)]$^+$}, 1051 {[M − 2 THF − 2($FeCl_4$)]$^+$}, 945 {[M − 3THF − Cl]$^+$}. MS (low-resolution electrospray)$^-$ (3.36 × 10^6 V) (*m*/*z*): 197.8 {[$FeCl_4$]$^-$}.

Synthesis of [Fe_6(L^1)$_2$(μ-OMe)$_6$(μ_4-O)$_2$$Cl_4$] (3). Solid NaH (0.279 g, 1.16 mmol, after washing the with pentane under nitrogen) was added to a solution of H_2L^1 (0.133 g, 0.37 mmol) in THF (5 mL). The resulting cloudy suspension was stirred under nitrogen for 2 h. A solution of $FeCl_3$ (0.056 g, 0.35 mmol) in dry degassed THF (5 mL) was then added and the clear yellow solution stirred under nitrogen for 10 min. A solution of $FeCl_3$ (0.112 g, 0.69 mmol) in dry MeOH (5 mL) was added to the reaction mixture, which was stirred in the air for 2 h. Orange crystals of **3** were obtained by cooling the reaction mixture to −23 °C for 8 weeks. Yield: 0.029 g, 12%. Anal. Found: C, 33.59; H, 4.49; 9.89. Calcd for $C_{40}H_{64}N_{10}O_{16}Cl_4Fe_6$: C, 33.85; H, 4.51; 9.87. IR (ν_{max}, cm^{-1}): 2960, 2928, 2872 (C−H), 2823 (C−H from O−CH_3), 1636 (C═O), 1576 (C═C), 1542 (C═N). FAB-MS$^+$ (*m*/*z*): 1348 [M − 2Cl].

Synthesis of [Fe_3(L^1)$_3$(μ_3-O)] (4). DBU (1,8-diazabicyclico-[5.4.0]undec-7-ene) (0.082 mL, 0.6 mmol) was added to a solution of H_2L^1 (0.103 g, 0.29 mmol) in THF (20 mL). The resulting solution was stirred for ca. 15 min, after which time it was filtered. $FeCl_2$ (0.035 g, 0.28 mmol) was then added as a solid and the mixture stirred. Upon addition of the metal the solution (which was open to air) immediately changed color from colorless to deep blue and a small amount of sticky precipitate formed. The blue solution was then stirred for ca. 3 h and filtered to remove the precipitate. The remaining solution was concentrated under reduced pressure and a blue product (**4**) obtained by precipitation with hexane. Purification was achieved by recrystallization from warm diethyl ether. Anal. Found: C, 48.42 H, 5.40; N, 16.55. Calcd for $C_{51}H_{69}Fe_3N_{15}O_{13}$: C, 48.32; H, 5.49; N, 16.57. IR (ν_{max}/cm^{-1}, KBr): 2957 (C−H), 2931 (C−H), 2870 (C−H), 1630 (C═O), 1592 (C═N), 1550, 1354, 779 (Fe_3O). MS (FAB$^+$) (*m*/*z*): 1266 {[Fe_3L_3O]$^+$}, 1194 {[Fe_2L_3]$^+$}.

Synthesis of [Fe_3(L^2)$_3$(μ_3-O)] (5). DBU (1,8-diazabicyclico-[5.4.0]undec-7-ene) (0.097 mL, 0.7 mmol) was added to a solution of H_2L^2 (0.101 g, 0.33 mmol) in THF (20 mL). The resulting solution was stirred for ca. 15 min, after which time it was filtered. $FeCl_2$ (0.042 g, 0.33 mmol) was then added as a solid and the mixture stirred. Upon addition of the metal salt the solution (which was open to air) immediately changed color from colorless to deep blue and a small amount of sticky precipitate formed. The blue solution was then stirred for ca. 3 h and filtered to remove the precipitate. The remaining solution was concentrated under reduced pressure and a blue product (**5**) obtained by precipitation with hexane. Single crystals suitable for X-ray analysis were obtained from CH_2Cl_2/diethyl ether. IR (ν_{max}/cm^{-1}, KBr): 2962 (C−H), 2924 (C−H), 2872 (C−H), 1632 (C═O), 1590 (C═N), 1540, 1354, 776 (Fe_3O). MS (FAB$^+$) (*m*/*z*): 1099 {[Fe_3L_3O]$^+$}, 1055 {[Fe_2L_3]$^+$}.

Magnetic Measurements. Low-field magnetic measurements were performed using a Quantum Design MPMS2 SQUID magnetometer at The University of Edinburgh. Measurements up to fields of 7 T were performed using an MPMS7 SQUID magnetometer at The Royal Institution of Great Britain and a Quantum Design physical properties measurement system at The University of Edinburgh.

Results and Discussion

Synthesis of H_2L^n and Structural Characterization of H_2L^1. As described in a preliminary communication,[2] *N*,*N*′-bis(*n*-butylcarbamoyl)pyridine-2,6-dicarboxamide (H_2L^1) was prepared from the reaction of 2,6-pyridinedicarbonyl dichloride with a 2-fold excess of butylurea in CH_2Cl_2 to yield H_2L^1 in 76% yield. The product was characterized by NMR and IR spectroscopies and the formulation confirmed by elemental analyses. To determine its hydrogen-bonding properties in the solid state, the product was structurally characterized by X-ray crystallography (Figure 1). An analogous procedure was used to synthesize H_2L^2, which was also characterized by NMR and IR spectroscopies and the formulation confirmed by elemental analyses.

The free ligand H_2L^1 crystallizes as hydrogen-bonded dimer pairs (see Figure 1), the two independent molecules (**A** and **B**, the latter being labeled with primes) being related by an approximate C_2 axis of symmetry (see Table 1). Both

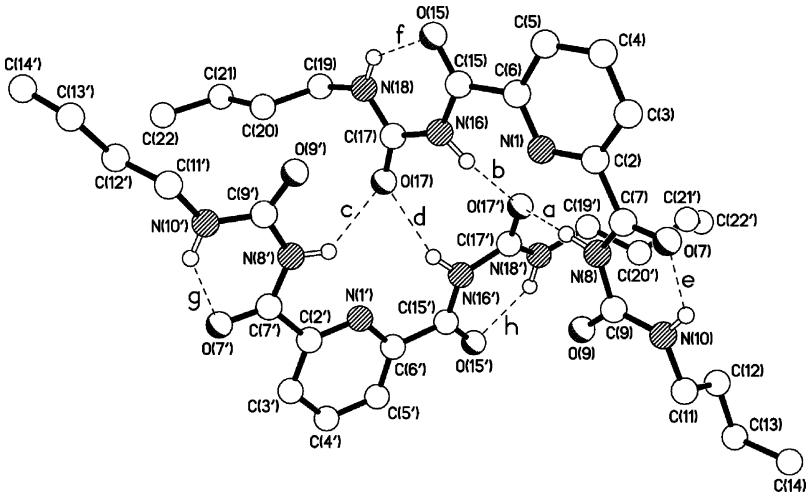

Figure 1. One of the hydrogen-bonded dimer pairs in the structure of $\mathbf{H_2L^1}$. The N−H···O hydrogen bonds have the following N···O and H···O lengths (Å) and N−H···O angles (deg): (a) 3.038(4), 2.23, 149; (b) 2.946(4), 2.17, 145; (c) 3.177(5), 2.46, 137; (d) 2.963(5), 2.15, 150; (e) 2.729(4), 2.04, 133; (f) 2.693(5), 1.95, 138; (g) 2.683(6), 1.95, 137; (h) 2.723(5), 1.98, 139.

Table 1. Crystallographic Data for Compounds $\mathbf{H_2L^1}$, **3**, and **5**[a] (CCDC 251541−251543)

data	$\mathbf{H_2L^1}$	**3**	**5**
chem formula	$C_{17}H_{25}N_5O_4$	$C_{40}H_{64}N_{10}O_{16}Cl_4Fe_6$	$C_{39}H_{45}Fe_3N_{15}O_{13}$
solvent		H_2O	
fw	363.42	1435.96	1099.45
T (°C)	20	−100	20
space group	$C2/c$ (No. 15)	$C2/c$ (No. 15)	$Pbcn$ (No. 60)
a (Å)	24.0740(10)	29.052(8)	19.754(4)
b (Å)	9.7147(3)	21.790(6)	12.848(2)
c (Å)	33.303(2)	10.205(2)	18.185(4)
α (deg)			
β (deg)	97.854(4)	98.36(2)	
γ (deg)			
V (Å^3)	7715.6(6)	6391(3)	4615.4(15)
Z	16[b]	4[c]	4[d]
ρ_{calcd} (g cm^{-3})	1.251	1.492	1.582
λ (Å)	1.541 78	1.541 78[e]	0.710 73
μ (mm^{-1})	0.752	12.736	1.011
R_1[f]	0.063	0.087	0.049
wR_2[g]	0.169	0.189	0.098

[a] Siemens P4 diffractometer, graphite-monochromated Mo Kα radiation, and refinement based on F^2. [b] There are two crystallographically independent molecules. [c] The molecule has crystallographic C_i symmetry. [d] The molecule has crystallographic C_2 symmetry. [e] Rotating anode source. [f] $R_1 = \Sigma||F_o| - |F_c||/\Sigma|F_o|$. [g] $wR_2 = \{\Sigma[w(F_o^2 - F_c^2)^2]/\Sigma[w(F_o^2)^2]\}^{1/2}$; $w^{-1} = \sigma^2(F_o^2) + (aP)^2 + bP$.

molecules have very similar conformations with an rms deviation for their best fit (excluding their *n*-butyl chains) of ca. 0.2 Å. In each molecule the central pyridyl ring and its adjacent pairs of trans amide groups are approximately coplanar with maximum out-of-plane torsional twists of ca. 16 and 14° about the C(2)−C(7) and N(16′)−C(17′) bonds, respectively. Each of the four amide groups exhibits a typical pattern of bond delocalization, while the C−N bond linking each pair [i.e. N(8)−C(9), N(16)−C(17), etc.] is of normal single bond length averaging ca. 1.41 Å (Table 2). The only interdimer packing interaction of note is between centrosymmetrically related pairs where the C(15)═O(15) bond (of molecule **A**) in one dimer overlays the center of the N(1)-containing pyridyl ring of the other (again in molecule **A**), and vice versa; the bond-centroid···ring-centroid separation is 3.37 Å with the linking vector being inclined by 82° to the ring plane.

Table 2. Selected Bond Lengths (Å) for $\mathbf{H_2L^1}$

	mol **A**	mol **B**		mol **A**	mol **B**
C(2)−C(7)	1.501(6)	1.502(6)	C(7)−O(7)	1.229(5)	1.219(5)
C(7)−N(8)	1.356(5)	1.351(6)	N(8)−C(9)	1.408(5)	1.417(6)
C(9)−O(9)	1.232(5)	1.218(6)	C(9)−N(10)	1.319(5)	1.319(7)
N(10)−C(11)	1.455(5)	1.441(6)	C(6)−C(15)	1.503(6)	1.480(6)
C(15)−O(15)	1.220(5)	1.229(5)	C(15)−N(16)	1.357(5)	1.360(5)
N(16)−C(17)	1.408(5)	1.397(6)	C(17)−O(17)	1.227(5)	1.232(5)
C(17)−N(18)	1.321(5)	1.328(6)	N(18)−C(19)	1.452(5)	1.434(6)

The dimeric $\mathbf{H_2L^1}$···$\mathbf{H_2L^1}$ pairs observed in the solid-state structure seem to be also present in solution. The electrospray mass spectrum of a sample of the ligand indicated an intense peak at 727 amu corresponding to two molecules of $\mathbf{H_2L^1}$; the peak associated with one molecule of $\mathbf{H_2L^1}$ (364 amu) was also observed clearly.

Reactions of $\mathbf{H_2L^1}$ with Iron Chloride. As we have described previously,[2] the reaction of 2 equiv of $\mathbf{H_2L^1}$ (in CH_2Cl_2) with a one-to-one mixture of $FeCl_2$ and $FeCl_3$ yielded the novel quadruply stranded helicate $[Fe_2(\mu\text{-}\mathbf{H_2L^1})_4(\mu\text{-}Cl)_2][FeCl_4]_2$ (**1**). The role of $FeCl_3$ in this reaction is as a chloride abstractor yielding an iron(II) dinuclear core with $[FeCl_4]^-$ counterions (see the magnetism section below). Interestingly, when the above reaction was repeated in THF the metallamacrocycle $[Fe_2(\mu\text{-}\mathbf{H_2L^1})_2(THF)_4Cl_2][FeCl_4]_2$ (**2**) was formed instead of the helicate **1**. The X-ray crystal structures of both **1** and **2** were previously reported[2] confirming the above formulations.

These results indicated the versatility of $\mathbf{H_2L^1}$ as a ligand for coordination to iron centers. Consequently, we engaged in studying the products that would result from the reaction of the bis-deprotonated form of the ligand and iron chloride. It has been previously established by Mascharak[3] that iron forms stable complexes with carboxamido donor ligands (formed upon deprotonation of −NH(C═O)R groups). In the case of $\mathbf{H_2L^1}$, the presence of the −NHC(═O)NHC(═O)-

(3) Marlin, D. S.; Mascharak, P. K. *Chem. Soc. Rev.* **2000**, *29*, 69.

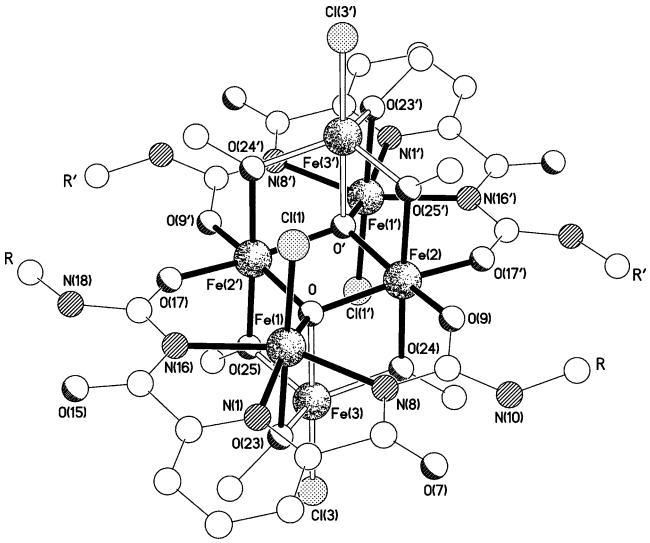

Figure 2. Molecular structure of **3** (R, R′ = *n*-Bu).

NH−R groups in positions 2 and 5 of the pyridine ring could provide an N,N′,N″ dinegative ligand to coordinate the iron center but still retain −C(═O)NH−R moieties for further hydrogen-bonding and/or metal−ligand interactions.

Several reactions varying the solvents, oxidation state of the iron, the iron-to-ligand ratios, and reaction times were carried out. The reaction mixtures produced in these reactions were complex and not easy to characterize. However, when $\mathbf{H_2L^1}$ was treated with 2 equiv of NaH (with the aim of deprotonating the two −C(═O)NH−R groups directly attached to the pyridine ring) and mixed with 6 equiv of $FeCl_3$ in THF/MeOH, the unexpected hexairon cluster $[Fe_6(\mathbf{L^1})_2(\mu\text{-OMe})_6(\mu_4\text{-O})_2Cl_4]$ (**3**) was formed. This product was obtained as orange crystals after the reaction mixture was filtered and the filtrate kept at −23 °C for several weeks (the first crystals appeared after 48 h). The product was characterized on the basis of spectroscopic, analytical, and structural techniques.

Spectroscopic and Structural Characterization of 3. A single-crystal X-ray analysis revealed the formation of a centrosymmetric hexanuclear iron complex (Figure 2). The structure can be envisaged as comprising two iron centers [type 1, Fe(1)] each of which exhibit the expected tridentate N,N′,N″ coordination to the "bis(urea−pyridyl)" ligand. The remaining octahedral sites on each center are occupied by axial chloride and methoxy ligands and in the fourth equatorial site by an oxo ligand (which is likely to come from traces of H_2O in the reaction mixture). These two units are bridged by two other iron atoms [type 2, Fe(2)] which coordinate to the oxo ligands on the "type 1" iron centers and also to two urea oxygen atoms from different "bis(urea−pyridyl)" ligands. The hexacoordination geometry on these two (type 2) iron centers is completed by methoxy groups. The axially positioned methoxy groups on both the "type 1" and "type 2" iron centers together with the bridging oxo ligands provide an optimal environment for the coordination of yet another pair of iron centers [type 3, Fe(3)]. These latter iron atoms complete their pentacoordination with one "axial" chloride each.

Table 3. Selected Bond Lengths (Å) and Angles (deg) for **3**

Fe(1)−O	1.873(9)	Fe(1)−Cl(1)	2.283(5)
Fe(1)−N(1)	2.085(12)	Fe(1)−N(8)	2.168(12)
Fe(1)−N(16)	2.138(12)	Fe(1)−O(23)	2.170(11)
Fe(2)−O	2.011(10)	Fe(2)−O′	2.010(10)
Fe(2)−O(9)	1.979(11)	Fe(2)−O(17′)	1.967(11)
Fe(2)−O(24)	1.993(10)	Fe(2)−O(25′)	2.030(10)
Fe(3)−O	2.153(9)	Fe(3)−Cl(3)	2.244(5)
Fe(3)−O(23)	1.911(10)	Fe(3)−O(24)	1.924(11)
Fe(3)−O(25)	1.912(11)		
O−Fe(1)−N(1)	161.2(4)	O−Fe(1)−N(16)	104.7(4)
N(1)−Fe(1)−N(16)	75.7(5)	O−Fe(1)−N(8)	101.6(4)
N(1)−Fe(1)−N(8)	75.6(5)	N(16)−Fe(1)−N(8)	151.2(5)
O−Fe(1)−O(23)	77.5(4)	N(1)−Fe(1)−O(23)	83.8(4)
N(16)−Fe(1)−O(23)	87.5(4)	N(8)−Fe(1)−O(23)	86.9(4)
O−Fe(1)−Cl(1)	98.7(3)	N(1)−Fe(1)−Cl(1)	100.1(3)
N(16)−Fe(1)−Cl(1)	92.9(4)	N(8)−Fe(1)−Cl(1)	94.6(3)
O(23)−Fe(1)−Cl(1)	176.1(3)	O(17′)−Fe(2)−O(9)	96.1(4)
O(17′)−Fe(2)−O(24)	88.4(4)	O(9)−Fe(2)−O(24)	90.5(5)
O(17′)−Fe(2)−O	93.1(4)	O(9)−Fe(2)−O′	163.9(4)
O(24)−Fe(2)−O′	103.0(4)	O(17′)−Fe(2)−O	163.6(4)
O(9)−Fe(2)−O	95.0(4)	O(24)−Fe(2)−O	79.4(4)
O′−Fe(2)−O	79.2(4)	O(17′)−Fe(2)−O(25′)	90.3(4)
O(9)−Fe(2)−O(25′)	87.1(5)	O(24)−Fe(2)−O(25′)	177.1(5)
O′−Fe(2)−O(25′)	79.6(4)	O−Fe(2)−O(25′)	102.4(4)
O(23)−Fe(3)−O(25)	113.7(4)	O(23)−Fe(3)−O(24)	120.3(5)
O(25)−Fe(3)−O(24)	112.9(5)	O(23)−Fe(3)−O	77.2(4)
O(25)−Fe(3)−O	78.7(4)	O(24)−Fe(3)−O	77.5(4)
O(23)−Fe(3)−Cl(3)	101.2(4)	O(25)−Fe(3)−Cl(3)	102.5(3)
O(24)−Fe(3)−Cl(3)	103.0(3)	O−Fe(3)−Cl(3)	178.3(3)
Fe(1)−O−Fe(2′)	125.6(4)	Fe(1)−O−Fe(2)	125.5(5)
Fe(2′)−O−Fe(2)	100.8(4)	Fe(1)−O−Fe(3)	103.5(4)
Fe(2′)−O−Fe(3)	96.7(4)	Fe(2)−O−Fe(3)	96.7(3)

The geometry at Fe(1) is appreciably distorted with cis angles ranging between 75.6(5) and 104.7(4)° and trans angles of 151.2(5) (the bite of the tridentate ligand), 161.2(4), and 176.1(3)°. The Fe−O separation of 1.873(9) Å suggests a distinct degree of multiple bond character in this bond; the other linkages are unexceptional (Table 3).

The coordination at Fe(2) is also distorted octahedral with cis angles ranging between 79.2(4) and 103.0(4)° and trans angles of 163.6(4), 163.9(4), and 177.1(5)°. All of the Fe−O linkages are unexceptional, ranging between 1.967(11) and 2.030(10) Å.

The coordination at Fe(3) can be considered as flattened tetrahedral [angles in the range 101.2(4)−120.3(5)°] with an additional longer contact through the base "trans" to the chloro substituent to give a distorted trigonal bipyramidal arrangement about this center. The iron center lies 0.41 Å out of the base formed by the three bridging methoxy groups, and the Fe−O distances are in the range 1.911(10)−1.924(11) Å; the distance to the bridging oxo ligand that approaches through this base is 2.153(9) Å.

The geometry at the tetrabridging oxo ligands is flattened tetrahedral [angles in the range 96.7(4)−125.6(4)°], the oxygen lying only 0.32 Å out of the {Fe(1),Fe(2),Fe(2A)} plane. This geometry contrasts with that observed in the related hexanuclear iron complex[4] $[Fe_6(\mu^4\text{-O})_2(\mu\text{-OMe})_8(\text{OMe})_4(\text{tren})_2]^{2+}$, where the geometry at the oxo centers approaches orthogonal (i.e. resembling an octahedral geometry where two cis sites are unoccupied).

The molecular structure of **3** revealed by X-ray crystallography is consistent with the spectroscopic and analytical

(4) Nair V. S.; Hagen, K. S. *Inorg. Chem.* **1992**, *31*, 4048.

data of the bulk sample. The FAB(+) mass spectrum of **3** revealed a peak at 1348 amu (corresponding to **3** − 2Cl). The IR spectrum shows several sharp bands between 2960 and 2872 cm^{-1} (C−H of the *n*-butyl groups of L), one at 2823 cm^{-1} (C−H of the bridging methoxy groups), a strong band at 1636 cm^{-1} (C═O), and strong bands at 1576 and 1542 cm^{-1} (C═N and C═C from pyridine). The elemental analyses of several crops of the crystals were also consistent with the above formulation. No further characterization of **3** was attempted since, once it crystallizes, this compound is insoluble in all common solvents.

In this reaction, the formation of the expected N,N′,N″-coordinated [Fe$\mathbf{L^1}$] fragment was indeed achieved. However, the structure of the product isolated indicates that this fragment is very reactive toward both H_2O and MeOH, which are incorporated as bridging ligands between the iron centers. It is important to note that the hexanuclear compound **3** was initially obtained using a 1:1 stoichiometry between $FeCl_3$ and the ligand. However, in the final isolated product, there are only two ligands and six iron atoms. This is likely to be a consequence of the uncompleted deprotonation of the ligand by NaH and of the relatively high reactivity of the [Fe$\mathbf{L^1}$] species formed in the reaction mixture. This metal−ligand fragment has the ability to react with H_2O and MeOH and also to coordinate to other iron centers using the two free C═O groups on the ligand.

Although the hexairon complex **3** was obtained unexpectedly, it is of interest in the context of polyiron−oxo compounds. Generally, the hydrolysis of iron results in the formation of insoluble polyiron−oxo compounds[5] unless capping ligands are present to control the growth process yielding soluble molecular aggregates.[6] These polynuclear iron complexes are important due to their unique magnetic properties,[7] besides being potentially useful models for the biomineralization process of this metal.[8] Although capping ligands have been previously used to prepare several soluble polynuclear iron complexes,[6] the present compound represents a new example of how a capping ligand can control the nuclearity of the final product. As will be discussed in the next section, by changing some of the experimental conditions and reagents of the current system, it is possible to obtain yet another molecular polyiron−oxo compound.

Synthesis and Characterization of 4 and 5. Due to the difficulties in controlling the deprotonation of the ligand using NaH (which is difficult to weigh out accurately since it needs to be washed from the oil in which it is suspended prior to use) it was decided to use a different base (namely DBU) to deprotonate the ligand and investigate the reaction of $\mathbf{[L_1]^{2-}}$ with iron chloride. A solution of $\mathbf{H_2L^1}$ in THF was first treated with 2 equiv of DBU to obtain the bis-deprotonated ligand. Addition of $FeCl_2$ to this solution (in the presence of oxygen) caused an immediate color change from colorless to dark blue. The reaction mixture was stirred for 3 h, filtered, and concentrated under reduced pressure; addition of hexane to this solution yielded a dark blue crystalline material which was separated and characterized on the basis of spectroscopic and analytical techniques as $[Fe_3(\mathbf{L^1})_3(\mu_3\text{-O})]$ (**4**). Particularly indicative of the above formulation was the FAB(+) mass spectrum, which showed a peak at 1266 amu that corresponds to three iron centers, three ligands, and one oxygen atom. This formulation was confirmed by elemental analyses.

To establish the exact structure of this new species, several attempts to grow single crystals for an X-ray analysis were made. Unfortunately, none of the crystals obtained provided good enough crystallographic data to determine the structure of the species. To overcome this problem and be able to obtain a crystal structure of the trinuclear iron complex it was then decided to prepare $\mathbf{H_2L^2}$—the ethyl analogue of $\mathbf{H_2L^1}$—and use it as a ligand to obtain the corresponding triiron compound. When the butyl substituents of the ligand were changed to ethyl groups, it was hoped that the solubility and crystallinity properties of the complex would be modified so that a structural determination would be possible.

This ligand was deprotonated with DBU and then mixed with $FeCl_2$ (following an analogous procedure described above for the reaction between $FeCl_2$ and $\mathbf{H_2L^1}$) to yield a dark blue product that was isolated and then characterized on the basis of structural and spectroscopic techniques as the mixed-valence complex $[Fe_3(\mathbf{L^2})_3(\mu_3\text{-O})]$ (**5**). Single crystals of this trinuclear compound suitable for X-ray crystallographic analysis were obtained from a mixture of CH_2Cl_2 and diethyl ether.

The X-ray analysis of **5** confirmed the formation of a (μ_3-oxo)triiron complex proposed for both **4** and **5**, with each ligand utilizing five of its seven potential binding sites (Figure 3).

The complex has a propeller-like conformation with crystallographic C_2 symmetry (about the Fe(2)−O bond) and, excluding the terminal methyl groups, approximate molecular D_3 symmetry. In each ligand the pairs of amide groups are approximately coplanar with the pyridyl ring, the largest out-of-plane torsional twists being 7 and 13° about the N(8)−C(9) and N(28)−C(29) bonds, respectively. The pattern of bonding within the ligands does not differ significantly from that observed in the *n*-butyl structure $\mathbf{H_2L^1}$. Each noncoordinated nitrogen center is intramolecularly hydrogen bonded to the carbonyl oxygen atom of its adjacent amide group; the N···O distances are in the range 2.624(6)−2.641(6) Å. The geometry at each iron center is distorted octahedral with cis angles in the range 75.32(15)−104.57(14)° at Fe(1) and 75.99(11)−104.01(11)° at Fe(2). The acute angles are in each case associated with the N,N bite of each five-membered chelate ring; the N(8)−Fe(1)−N(14) and N(28)−Fe(2)−N(28A) angles are 151.71(15) and 152.0(2)°, respectively. The metal coordination distances are unexceptional though

(5) (a) Schneider, W. *Comments Inorg. Chem*. **1984**, *3*, 205. (b) Lippard, S. J. *Angew. Chem., Int. Ed. Engl.* **1988**, *27*, 344. (c) Kurtz, D. M. *Chem. Rev*. **1990**, *90*, 585.
(6) (a) Caneschi, A.; Cornia, A.; Lippard, S. J. *Angew. Chem., Int. Ed. Engl*. **1995**, *34*, 467 and references therein. (b) Grant, C. M.; Knapp, M. J.; Streib, W. E.; Huffman, J. C.; Hendrickson, D. N.; Christou, G. *Inorg. Chem*. **1998**, *37*, 6065.
(7) (a) Benelli, C.; Cano, J.; Journaux, Y.; Sessoli, R.; Solan, G. A.; Winpenny, R. E. P. *Inorg. Chem*. **2001**, *40*, 188. (b) Cannon, R. D.; White, R. P. *Prog. Inorg. Chem*. **1988**, *36*, 195.
(8) (a) Hagen, K. S. *Angew. Chem., Int. Ed. Engl*. **1992**, *31*, 1010. (b) Taft, K. L.; Papaefthymiou, G. C.; Lippard, S. J. *Inorg. Chem*. **1994**, *33*, 1510.

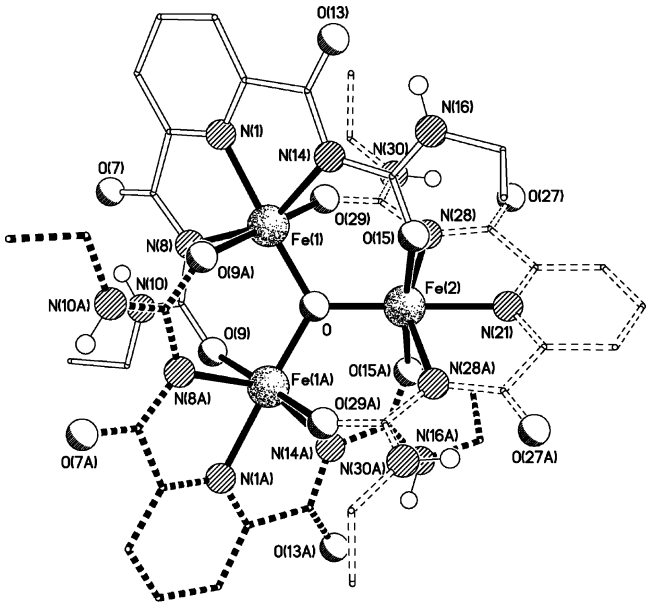

Figure 3. Molecular structure of the triiron complex **5**.

Table 4. Selected Bond Lengths (Å) and Angles (deg) for **5**

Fe(1)−O	1.873(2)	Fe(1)−N(1)	2.081(4)
Fe(1)−N(8)	2.160(4)	Fe(1)−O(9A)	2.126(3)
Fe(1)−N(14)	2.184(4)	Fe(1)−O(29)	2.130(3)
Fe(2)−O	1.822(4)	Fe(2)−O(15)	2.054(3)
Fe(2)−N(21)	2.085(5)	Fe(2)−N(28)	2.140(4)
O−Fe(1)−N(1)	177.37(16)	O−Fe(1)−O(9A)	90.78(13)
N(1)−Fe(1)−O(9A)	91.68(15)	O−Fe(1)−O(29)	89.74(12)
N(1)−Fe(1)−O(29)	87.87(15)	O(9A)−Fe(1)−O(29)	176.17(15)
O−Fe(1)−N(8)	104.57(14)	N(1)−Fe(1)−N(8)	76.46(16)
O(9A)−Fe(1)−N(8)	87.45(15)	O(29)−Fe(1)−N(8)	88.74(14)
O−Fe(1)−N(14)	103.54(14)	N(1)−Fe(1)−N(14)	75.32(15)
O(9A)−Fe(1)−N(14)	95.36(15)	O(29)−Fe(1)−N(14)	88.21(15)
N(8)−Fe(1)−N(14)	151.71(15)	O−Fe(2)−O(15)	93.50(11)
O(15)−Fe(2)−O(15A)	173.0(2)	O−Fe(2)−N(21)	180
O(15)−Fe(2)−N(21)	86.50(10)	O−Fe(2)−N(28)	104.01(11)
O(15)−Fe(2)−N(28)	90.83(15)	N(21)−Fe(2)−N(28)	75.99(11)
O(15)−Fe(2)−N(28A)	87.47(15)	N(28)−Fe(2)−N(28A)	152.0(2)
Fe(1)−O−Fe(2)	119.83(12)	Fe(1)−O−Fe(1A)	120.3(2)

it is noticeable that the Fe(1)−O bond lengths are all significantly longer than those for Fe(2)−O (Table 4) suggesting a higher oxidation state for Fe(2) than Fe(1). As there are no counterions in the structure, to balance the charges the complex must contain either one iron(II) and two iron(III) centers or one iron(III) and two iron centers with a valence between Fe^{II} and Fe^{III}. This could be explained by proposing a system where there is a degree of delocalization providing a +2.5 oxidation state on each of the two iron centers. Alternatively, since Fe(1) and Fe(1A) are crystallographically related, it is more likely that the system is a case of statistical disorder of trapped-valence Fe^{II}/Fe^{III} and Fe^{III}/Fe^{II}. If one considers the Fe−oxo distances we have two "long" [1.873(2) Å] and one "short" [1.822(4) Å] bonds. In literature examples[9,10] of related (μ_3-oxo)tris(pyridine)-triiron(III) cations the Fe−oxo distances range between 1.903 and 1.916 Å. In analogous neutral, mixed oxidation complexes containing one iron(II) and two iron(III) centers the pattern of Fe−oxo bonding is not consistent, with some complexes containing, as in **5**, two "long" and one "short" Fe−O bonds[11,12] whereas others have two "short" and one "long" Fe−O bonds.[13,14] Clearly, therefore, this parameter alone is not a reliable guide to the oxidation state of the metal.

To get a better idea of the oxidation states of the three iron centers a bond valence sum (BVS) analysis was carried out using the parameters provided by Thorp.[15] This analysis showed that the Fe(1) and Fe(1A) centers are consistent with a partial oxidation state of 2.5 (the BVS being 2.45) while Fe(2) is in oxidation state +3 (the BVS being 3.09).[16] These values would be consistent with the observed Fe−O distances and with the proposal of having a system with static disorder of trapped-valence Fe^{II}/Fe^{III} and Fe^{III}/Fe^{II} (as discussed in the previous paragraph).

Magnetic Measurements of 1−4. The magnetic properties of **1** and **2** were investigated by variable-temperature magnetization measurements over the temperature range 2−300 K. For both complexes, the data above 35 K were fit to the Curie−Weiss expression to give a Curie constant of 17.9 emu K mol^{-1} (**1**) and 16.9 emu K mol^{-1} (**2**) with a Weiss constant of −2.3 K (**1**) and −7.1 K (**2**) indicative of predominant weak antiferromagnetic interactions in each case. A Curie constant of 14.75 would be predicted for 2 × Fe^{3+} counterions plus 2 × Fe^{2+} centers using a spin-only formula. Since some orbital contribution to the magnetic moment would be expected for the d^6 six-coordinate Fe^{2+} centers, the values of the Curie constant observed are consistent with a value larger than the spin-only formula. It should be noted however that a Curie constant of 17.5 emu K mol^{-1} would be predicted for 4 × Fe^{3+} centers and magnetization measurements in this case are not a reliable indication of the oxidation state of the complexes, the assignment of which was more reliably achieved from the crystallographic data.[2]

The data for **1** and **2** were each also fit to a model for a dimer of two $S = 2$ Fe^{2+} centers[17] on the basis of Heisenberg spins, ignoring the effects of spin−orbit coupling and zero-field splitting. For both **1** and **2**, the iron(III)-containing counterions showed no short Fe···Fe distances or clear superexchange pathways among themselves or with the Fe^{2+} centers in the dimers. Thus, the fit also included the presence of two $g = 2$, $S = 5/2$ Fe^{3+} counterions using the assumption that these remained noninteracting throughout the tempera-

(9) Cui, Y.; Wang, Y.-M.; Zheng, Y.; Zhou, W.-B.; He, L.-J.; Cai, S.-H.; Chen, B.; Zhang, L.-N. *Chin. J. Struct. Chem*. **1999**, *18*, 51.
(10) Sowrey, F. E.; Tilford, C.; Wocadlo, S.; Anson, C. E.; Powell, A. K.; Bennington, S. M.; Montfrooij, W.; Jayasooriya, U. A.; Cannon, R. D. *J. Chem. Soc., Dalton Trans.* **2001**, 862.
(11) Manago, M.; Hayami, S.; Yano, Y.; Inoue, K.; Nakata, R.; Ishida, A.; Maeda, Y. *Bull. Chem. Soc. Jpn*. **1999**, *72*, 2229.
(12) Nakamoto, T.; Yoshida, M.; Kitagawa, S.; Katada, M.; Endo, K.; Sano, H. *Polyhedron* **1996**, *15*, 2131.
(13) Wu, C.-C.; Hunt, S. A.; Gantzel, P. K.; Gutlich, P.; Hendrickson, D. N. *Inorg. Chem*. **1997**, *36*, 4717.
(14) Overgaard, J.; Larsen, F. K.; Schiøtt, B.; Iversen, B. B. *J. Am. Chem. Soc*. **2003**, *125*, 11088.
(15) Liu, W.; Thorp, H. H. *Inorg. Chem*. **1993**, *32*, 4102.
(16) The bond valences (s) were calculated using the expression $s = \exp[(r_o - r)/B]$, where $B = 0.37$. The following r_o (Å) values reported by Thorp[15] were used: 1.765 for the Fe^{3+}−O bonds; 1.815 for the Fe^{3+}−N bonds; 1.700 for the Fe^{2+}−O bonds; 1.769 for the Fe^{2+}−N bonds.
(17) O'Connor, C. J. *Prog. Inorg. Chem*. **1982**, *29*, 203.

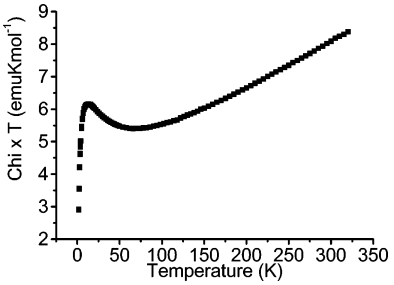

Figure 4. Temperature dependence of χT at a magnetic field of 100 G for the hexairon complex **3**.

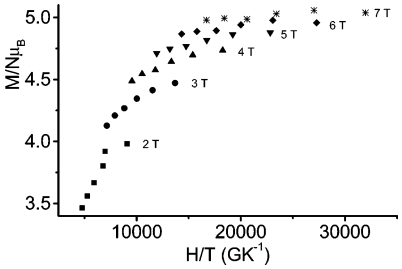

Figure 5. Reduced magnetization ($M/N\mu_B$) against H/T for applied fields of 2−7 T for the hexairon complex **3** (N = Avogadro's number, μ_B = the Bohr magneton, H = magnetic field).

ture range under study. This gave rise to coupling constants for **1** and **2** respectively of $J/k_B = -3.1$ and -3.6 K with $g = 2.4$ and 2.1. The presence of the counterions reduces the reliability of the fit for determination of the coupling constants in the dimer units. The magnetization for antiferromagnetically coupled dimers is expected to rise to a peak before dropping at low temperature; however, this occurs against a background of rising magnetization for the Fe^{3+} centers as temperature is reduced, leading to loss of accuracy in the determination of the peak magnetization of the dimer. Furthermore, the assumption of Heisenberg spins within the model requires that the value of the coupling constant is much larger than the zero-field splitting to be a good approximation, and this is not likely to be valid with such low values of J. The values determined, therefore, should be taken only as an indication that coupling within the dimer units is extremely weak.

It appears initially surprising that the coupling within **1** and **2** is similarly weak, given the very different structures of the two dinuclear complexes. The Fe···Fe separation in **2** is large (7.74 Å), and there are no obvious superexchange pathways except perhaps some $\pi-\pi$ interaction between the amide units of the ligand. Thus, in this case, the lack of any strong coupling is not surprising. In addition, however, dinuclear iron(II)−iron(II) complexes with two alkoxy bridges have typically shown weak coupling that may be either ferro- or antiferromagnetic.[18−20] Thus, in this light, it is also consistent with prior observations that **1**, with the related $(\mu\text{-Cl})_2$ briding motif, also shows only very weak coupling between the Fe^{2+} centers.

The magnetic properties of the hexairon complex **3** were investigated by variable-temperature dc and ac magnetization measurements. These showed an initial fall of χT (Figure 4) with reducing temperature from a room-temperature value of 8.38 emu K mol^{-1}, considerably lower than the value expected for six noninteracting Fe^{3+} centers (26.28 emu K mol^{-1} with $g = 2$ and $S = 5/2$ per Fe^{3+} center), indicative of antiferromagnetic interactions within the cluster. At 14 K, χT again rises to a maximum of 6.14 emu K mol^{-1} suggesting a ground state with uncompensated alignment of the individual spins on the six Fe^{3+} centers. Below this temperature the value drops sharply, presumably due to intercluster interactions or zero-field splitting.

To investigate the ground-state spin of the cluster, the magnetization was studied in a SQUID magnetometer at high magnetic field. A plot of the reduced magnetization against H/T (Figure 5) indicates the magnetization saturates at a value of 5.04 μ_B, and the noncoincidence of the isofield data is consistent with the presence of some zero-field splitting of the ground state. To determine whether the species displays single-molecule magnet behavior, the ac susceptibility was recorded at frequencies from 30 to 1000 Hz and temperatures down to 2 K. The lack of any significant out-of-phase component of the susceptibility is taken as evidence that the species does not show single-molecule magnet behavior.

A ground-state intermediate between $S = 0$ ($M_{sat}/N\mu_B = 0$) and $S = 5$ ($M_{sat}/N\mu_B = 10$) is unexpected as it cannot be rationalized through parallel and antiparallel coupling of six individual $S = 5/2$ spin centers. To further verify this observation, high-field magnetization data were also recorded using ac magnetization measurement on a different instrument, and the results were consistent with a saturation magnetization of $M/N\mu_B \approx 5$. Iron(III) centers bridged by oxo and alkoxo units characteristically show antiferromagnetic coupling.[21] The molecular structure of the cluster, however, shows triangular arrangement of the iron(III) centers, and this may give rise to spin frustration since antiferromagnetic alignment of all neighboring spins is geometrically impossible.[22,23] In such a system, the magnetic behavior cannot necessarily be described by simple consideration of parallel and antiparallel spins, and possible intermediate value ground states may arise, depending on the ratio of the different coupling constants involved.[21−23] For six $S = 5/2$ Fe^{3+} centers, intermediate integral values of ground-state spin may therefore arise. The observed peak in the χT plot of 6.14 emu K mol^{-1} suggests the most likely ground state as $S = 3$, which would give a theoretical susceptibility maximum of 6 emu K mol^{-1} and saturation magnetization of $M/N\mu_B = 6$ for $g = 2$ metal centers.

An estimate of the magnetic exchange between oxygen-atom bridged Fe^{3+} centers can be given on the basis of an empirical relationship[21,24,25] that has been developed for

(18) Grillo, V. A.; Hanson, G. R.; Hambley, T. W.; Gahan, L. R.; Murray, K. S.; Moubaraki, B. *Dalton Trans*. **1997**, 305.
(19) Stassinopolous, A.; Schulte, G.; Papaefthymiou, G. C.; Caradonna, J. P. *J. Am. Chem. Soc*. **1991**, *113*, 8686.
(20) Snyder, B. S.; Patterson, G. S.; Abrahamson, A. J.; Holm, R. H. *J. Am. Chem. Soc*. **1989**, *111*, 5214.
(21) Gatteschi, D.; Caneschi, A.; Sessoli, R. *Chem. Soc. Rev*. **1996**, 101.
(22) McCusker, J. K.; Christmas, C. A.; Hagen, P. M.; Chadha, R. K.; Harvey, D. F.; Hendrickson, D. N. *J. Am. Chem. Soc.* **1991**, *113*, 6114.
(23) Libby, E.; McCusker, J. K.; Schmitt, E. A.; Folting, K.; Hendrickson, D. N.; Christou, G. *Inorg. Chem*. **1991**, *30*, 3486.
(24) Gorun, S. M.; Lippard, S. J. *Inorg. Chem*. **1991**, *30*, 1625.

binuclear systems and has also been applied to larger clusters.[26] This involves the assumption that the dominant exchange coupled pathway will be through the bridging oxygen ligand with the shortest average Fe−O bond length and that this single parameter can be used to predict the coupling constant *J*. Six different values of *J* are required to describe the coupling within the cluster,[27] and application of this model leads to values for these from −11.4 to −18.5 cm^{-1}. The small range of these *J* values would suggest that spin frustration effects may be manifest in the magnetic properties of the cluster. More recently, an alternative model for predicting exchange coupling has been developed using four hexanuclear iron compounds, involving some dependence on bridging angle as well as the shortest superexchange pathway.[28] Application of this model leads to a wider range of coupling constants from −3.3 to −18.5 cm^{-1} due to the variations in bridging angle. In this model J_{12} and $J_{12'}$ are much larger than $J_{22'}$, which would lead to opposing spins on Fe(2) and Fe(2′) compared with Fe(1) and Fe(1′).[28] The possibility for frustration however may still arise in the alignment of the spins on Fe(3) and Fe(3′), which show couplings to the other metals with a small range of values. Thus, overall, both the empirical model developed using dinuclear iron species and that developed using hexanuclear systems illustrate the possibility to observe a ground spin state intermediate between $S = 0$ and 5 with the most likely value from the recorded data as $S = 3$.

The magnetic susceptibility of **4** was studied over the temperature range 1.8−300 K, and a plot of χT against *T* (Figure 6) shows a reduction in χT with temperature, again consistent with predominantly antiferromagnetic interactions. This results in $\chi T = 3.92$ emu K mol^{-1} at room temperature, considerably lower than the value of 11.75 emu K mol^{-1} expected for two Fe^{3+} and one Fe^{2+} noninteracting centers. Magnetic analysis of related mixed-valent trinuclear iron systems has generally been carried out assuming trapped Fe^{2+} and 2 × Fe^{3+} valences. It was shown by Brown[30] that a model based on localized valences could successfully reproduce magnetic data, despite observation from Mössbauer results that his system undergoes dynamic intratrimer electron transfer. Since the iron sites in his complex were electronically distinguishable on some time scale, the system could be successfully treated as an Fe^{2+} plus 2 × Fe^{3+} trimer. We have initially explored this approach for **4** which has therefore been described using two coupling constants, that between Fe^{2+} and Fe^{3+} (*J*) and that between the two Fe^{3+} centers (*J*′). Ignoring the effects of spin−orbit coupling and zero-field splitting, a model for the temperature-dependent susceptibility can be developed using the methods of Kambe[29] and was previously determined for this system by Brown and co-workers.[30] Brown however stated that the susceptibility expression presented in his work differs in a number of terms from an earlier equation developed using the same methods by Lupu,[31] and due to this discrepancy, we redetermined the appropriate susceptibility equation using the standard procedures.[29] We found our susceptibility expression to be identical with that given by Brown in every term; however, it should be noted that the parameters $X = J/kT$ and $Y = J'/kT$ given in Brown's work[30] are incorrect as written and instead should be $X = -J/kT$ and $Y = -J'/kT$.

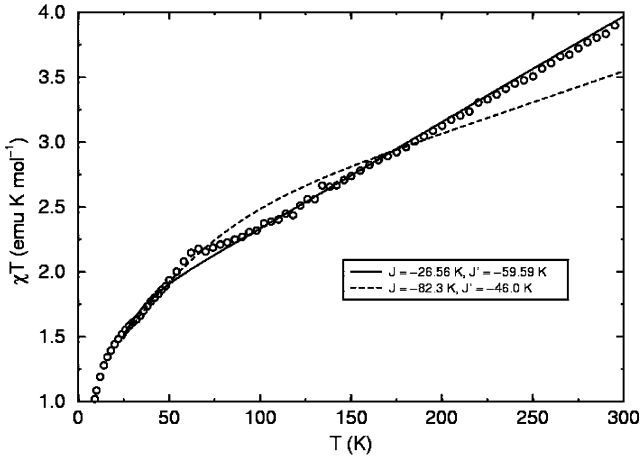

Figure 6. Temperature dependence of χT at a magnetic field of 100 G for the triiron complex **4**, showing fit over the temperature range 25−300 K giving two possible solutions: $J/k_B = -26.6$ K and $J'/k_B = -59.6$ K (solid line) or $J/k_B = -82.3$ K and $J'/k_B = -46.0$ K (broken line).

We were unable to fit this expression to the data over the entire temperature range, and this may be attributed to effects of spin−orbit coupling and zero-field splitting in the low-temperature region. The data were successfully fit however over the restricted range 25−300 K and led to two possible solutions, $J/k_B = -26.6$ K and $J'/k_B = -59.6$ K or $J/k_B = -82.3$ K and $J'/k_B = -46.0$ K, depending on the values used for the starting parameters in the fit. Studies of previous systems containing two Fe^{3+} centers and one Fe^{2+} center bridged by a central μ_3-oxygen atom in a triangular arrangement have largely shown *J* to be around three times larger than *J*′.[17] Thus, despite the clearly poorer fit for the latter values (see Figure 6), literature precedent would suggest that the fit with $J > J'$ represents the coupling within the complex. The significantly better fit with $J' > J$ that we observe may represent a genuine difference from literature precedent or

(25) Werner, R.; Ostrovsky, S.; Griesar, K.; Haase, W. *Inorg. Chim. Acta* **2001**, *326*, 78.
(26) Barra, A. L.; Caneschi, A.; Cornia, A.; Fabrizi de Biani, F.; Gatteschi, D.; Sangregorio, C.; Sessoli, R.; Sorace, L. *J. Am. Chem. Soc.* **1999**, *121*, 5302.
(27) (i) $J_{12} = -18.4$, $J_{12'} = -18.5$, $J_{22'} = -11.6$, $J_{31} = -11.4$, $J_{32} = -15.1$, and $J_{32'} = -16.5$ cm^{-1}, where J_{ab} = coupling between Fe(a) and Fe(b). All couplings are antiferromagnetic. Values are derived from the expression of Werner et al.[25] (a refinement of the method of Gorun and Lippard[24]), where $J = -10^7 \exp(-6.8P)$ and P = half the shortest superexchange pathway between the two metals. (ii) $J_{12} = -18.5$, $J_{12'} = -18.2$, $J_{22'} = -3.3$, $J_{31} = -3.9$, $J_{32} = -5.9$, and $J_{32'} = -6.0$ cm^{-1}, where J_{ab} = coupling between Fe(a) and Fe(b) (defined in Figure 2). Values are derived from the expression of Canada-Vilalta et al.,[28] where $J = 2 \times 10^7(0.2 - \cos\varphi + \cos^2\varphi)\exp(-7r)$, r = half the shortest superexchange pathway between the two metals, and φ = the Fe−O−Fe bridging angle. In keeping with the observations of Canada-Vilalta et al.,[28] we found that where multiple bridging oxygens were present, that with the shortest average Fe−O distance also showed the widest angle, and this pathway was used in the calculation.
(28) Canada-Vilalta, C.; O'Brien, T. A.; Brechin, E. K.; Pink, M.; Davidson, E. R.; Christou, G. *Inorg. Chem.* **2004**, *43*, 5505.
(29) (a) Sinn, E. *Coord. Chem. Rev.* **1970**, *5*, 313. (b) Kambe, K. *J. Phys. Soc. Jpn.* **1950**, *5*, 48.
(30) Dziobkowski, C. T.; Wrobleski, J. T.; Brown, D. B. *Inorg. Chem.* **1981**, *20*, 679.
(31) Lupu, D. *Rev. Roum. Chim.* **1970**, *15*, 417.

may arise due to limitations in the assumption of a valence-localized model.

Summary

The iron complexes discussed in this paper demonstrate the ability that the 2,5-disubstituted ligand $\mathbf{H_2L^1}$ has to form a wide range of polynuclear assemblies. By changing the solvent used in the reaction between a mixture of $FeCl_2$ and $FeCl_3$ with $\mathbf{H_2L^1}$ (from CH_2Cl_2 to THF), it is possible to obtain either the quadruply stranded helicate **1** (with CH_2Cl_2) or the macrocycle **2** (with THF). On the other hand, deprotonation of the carboxamide groups closer to the pyridine ring of the ligand has led to the formation of the unsaturated [Fe$\mathbf{L^1}$] species which readily reacts yielding the hexairon complex **3** or the triiron complex **4**. In the latter two structures, the ligand bridges several iron centers using the free C═O groups present in the ligands' substituents. The magnetic properties of the four complexes have been studied. Of particular interest is the behavior of the hexairon complex **3** which appears to be consistent with a zero-field split ground state with spin frustration playing a significant role in the properties observed.

Acknowledgment. We thank Imperial College London for a studentship (H.A.B.), the EPSRC for financial support, Philip Camp of The University of Edinburgh for assistance with data-fitting software, and Simon Carling and Ian Watts of The Royal Institution of Great Britain for recording the high-field magnetization data.

Supporting Information Available: X-ray crystallographic data in CIF format, figures of molecular structures, and tables of magnetic measurements. This material is available free of charge via the Internet at http://pubs.acs.org.

IC048620E